Translational Stroke Research (2019) 10:729–743
https://doi.org/10.1007/s12975-019-00702-1

ORIGINAL ARTICLE

Exploration of MST1-Mediated Secondary Brain Injury Induced by Intracerebral Hemorrhage in Rats via Hippo Signaling Pathway

Peng Zhang[1] · Tianyi Wang[1] · Dongping Zhang[1] · Zhuwei Zhang[1] · Shuai Yuan[1] · Juyi Zhang[1] · Jie Cao[1] · Haiying Li[1] · Xiang Li[1] · Haitao Shen[1] · Gang Chen[1]

Received: 28 May 2018 / Revised: 15 March 2019 / Accepted: 20 March 2019 / Published online: 2 April 2019

Abstract

Intracerebral hemorrhage (ICH) is a serious public health problem which causes high rates of disability and mortality in adults. Cell apoptosis is a sign of secondary brain injury (SBI) following ICH. Mammalian sterile 20-like kinase-1 (MST1), an apoptosis-promoting kinase, is a part of the Hippo signaling pathway and involved in cell death, oxidative stress, and inflammation. However, the role and underlying mechanism of MST1 in SBI induced by ICH have not yet been fully explained. The main purpose of present research was to explore the role of MST1 and its potential mechanism in SBI after ICH. An ICH model was established by injecting autologous blood into the right basal ganglia in male SD rats. We found that MST1 phosphorylation was significantly increased in brain tissues of rats after ICH. Additionally, inhibition of MST1 phosphorylation by a chemical inhibitor (Xmu-mp-1) and genetic knockdown could effectively reduce the activation of P-LATS1 and P-YAP which are downstream proteins of MST1 and decrease neuronal cell death and inflammation reaction in ICH rats. Furthermore, the decreased of MST1 phosphorylation reduced brain edema, blood-brain barrier (BBB) damage, and neurobehavioral impairment during ICH. Over-expression of MST1 resulted in opposite effects. Finally, deletion of MST1 significantly reduced neuronal apoptosis in vitro. In summary, our study revealed that MST1 played an important role in the SBI following ICH, and inhibition of MST1 could alleviate ICH-induced SBI. Therefore, MST1 may be considered as a potential therapeutic target for SBI following ICH.

Keywords MST1 · Intracerebral hemorrhage · Secondary brain injury · Neuronal apoptosis

Introduction

Intracerebral hemorrhage (ICH) is a global disease that accounts for 10–15% of all strokes annually, and is known for its high mortality and morbidity, as well as its dangerous course [1, 2]. The brain damage includes primary injury and secondary injury after ICH. Primary brain injury refers to the formation and expansion of intracerebral hematoma, causing mechanical damage to brain tissues [3]. In secondary brain injury (SBI), pathological changes include microglia activation, releasing of neurotransmitters and inflammatory mediators, brain edema, and blood-brain barrier (BBB) damage. These factors usually result in cell death (containing necrosis and apoptosis) in brain tissues [4]. Although potential treatments for SBI have been proposed, the clinical outcome of ICH patients remains unsatisfactory, with only about 20% of patients recover independent living of 6 months after ICH [5, 6]. Therefore, the regulatory mechanism of cell apoptosis after ICH merits further exploring.

Mammalian sterile 20-like kinase 1 (MST1), which is also called serine/threonine-protein kinase 4 (STK4) or stress response kinase 2 (SRK2), is a class II GC kinase belonging to the Ste-20 family. It contains 487 amino acid residues and has a molecular weight of 59 kD. The MST1 gene, a mammalian homolog of the Drosophila Hippo gene, is located in the human chromosome 20q11, and has a total length of 113 kb, containing 11 exons and 10 introns. Its DNA sequence

Peng Zhang, Tianyi Wang and Dongping Zhang contributed equally to this work.

✉ Haitao Shen
dagezi120@126.com

✉ Gang Chen
nju_neurosurgery@163.com

[1] Department of Neurosurgery & Brain and Nerve Research Laboratory, The First Affiliated Hospital of Soochow University, 188 Shizi Street, Suzhou 215006, Jiangsu Province, China

contains an open reading frame consisting of 1461 nucleotides, and the mRNA has a total length of 6344 bp. It is well known that the MST family contains four members: MST1/2/3 and MST4 [7]. MST1 is widely expressed in the most cells in the human body. As previously reported, it is well known that MST1 is the major member in the Hippo signaling pathway, which regulates biological size through adjusting cell proliferation and differentiation [8]. Many investigations have shown that MST1 participates in progression of inflammation, stress response, and cell apoptosis [9–11]. However, the physiological functions and mechanism of MST1 intracellular signaling are not yet clear. Considerable evidences suggested that MST1 also contributes to tissue damage and cell death. In 2003, four laboratories cloned and reported the function of the Hippo/MST gene [12–14]. In terms of neurodegenerative diseases, MST1 participates in amyotrophic lateral sclerosis (ALS) induced in a mouse model, suggesting that the Hippo pathway has an essential role in central nervous system (CNS) diseases [15]. In 2006, MST1-FOXO was found to be involved in nerve cell death induced by oxidative stress [16]. In 2011, it was also found that c-Abl may function upstream of MST1 to participate in nerve cell death [17]. In 2012, it was found that set9 could be used as a FOXO methylation modifier to participate in FOXO-induced neuronal death, expanding the epigenetic study of FOXO in the downstream of MST1 [18]. In 2015, MST1 was found to be involved in neuroinflammation caused by cerebral ischemia [19]. In 2018, it was found that genetic knockdown of MST1 reduces neuronal death and ameliorates neurological impairment in traumatic brain injury (TBI) in a rat model [20]. A previous report has indicated that the core of the Hippo pathway is a kinase cascade. MST1/2 and Sav1 kinase initially form a complex, and then LATS1/2 kinase is phosphorylated and activated. This in turn inhibits the transcription co-activator YAP/TAZ which are main downstream effectors in the Hippo pathway. When YAP/TAZ are dephosphorylated, they are transported to the nucleus and then interacted with TEAD1–4 and other transcription factors, thereby inducing cell proliferation and inhibiting apoptotic gene expression [21]. Taken these reports together, MST1 is associated with cell apoptosis in many CNS diseases. Since cell apoptosis exerts essential roles in SBI following ICH, we hypothesized that there may be an association between MST1 and cell apoptosis following ICH. Moreover, it has been reported that Src kinase, which is activated under ICH condition [22], can phosphorylate MST1. Phosphorylated MST1 can activate LATS1/2 kinase, which can then phosphate YAP/TAZ. When YAP/TAZ are phosphorylated, they are transported out of the nucleus and degraded, thereby inducing the apoptotic gene expression.

To date, no study reported the contribution of MST1 in brain injury induced by ICH, especially the effects of MST1-mediated Hippo signaling pathway during ICH. Therefore, the purpose of this research was to explore the effects of MST1 and assess the therapeutic potential of MST1 in ICH. In this work, we demonstrated that MST1 plays a role in SBI after ICH and that deletion of MST1 can effectively reduce neuronal cell death and inflammation, as well as alleviate BBB injury and brain edema in the ICH rat via regulation of the Hippo signaling pathway.

Materials and Methods

Animals and Ethic

Adult male Sprague Dawley (SD) rats weighing 280–300 g were purchased from the Animal Center of Chinese Academy of Sciences (Shanghai, China). The animal experimental protocols were approved by the Animal Care and Use Committee of Soochow University and performed in accordance with the National Institutes of Health guidelines. All experimental rats had adequate food and water, and they were housed in a humidity and temperature quiet-controlled environment under a regular light/dark schedule. In addition, we striped to reduce the use of animals and relieved their pain as much as possible.

Establishment of ICH Model In Vivo

An ICH model was established by injecting autologous blood into the right basal ganglia in rats as a previous report [23]. Briefly, for each rat in ICH group, firstly, it was anesthetized by intraperitoneal injection of 10% chloral hydrate. Its rectal temperature was maintained at 37 ± 0.5 °C by a feedback-controlled heating pad. The right femoral artery was catheterized to monitor arterial blood pressure and blood glucose levels. Secondly, it was placed and fixed with a three-dimensional positioning frame (ZH-Lanxing B-type stereotaxic frame, Anhui Zhenghua Biological Equipment Co. Ltd. China), and 100 μl autologous blood was obtained from its heart. Its scalp was exposed at 0.2 mm anterior to junction of coronary suture and the sagittal midline and 3.5 mm to right of sagittal suture to form a hole corresponding to basal ganglia. The microinjector was mounted on a stereotactic frame and the needle was slowly inserted (5.5 mm deep). Thirdly, the 100-μl autologous blood was slowly injected into its right basal ganglia (20 μl/min), and the needle was left at place for another 5 min. Then, the needle was slowly removed, and sterile bone wax was used to seal the hole in the skull. After confirming that there was no bleeding, the incision was sutured closed. Concomitantly, each rat in Sham group was just injected with an equivalent volume of physiological saline solution. Additionally, each rat in Normal group did not receive any surgical procedures. Schematic representation of brain coronal sections of three rats respectively from Normal group, Sham group, and ICH group was shown in Fig. 1a.

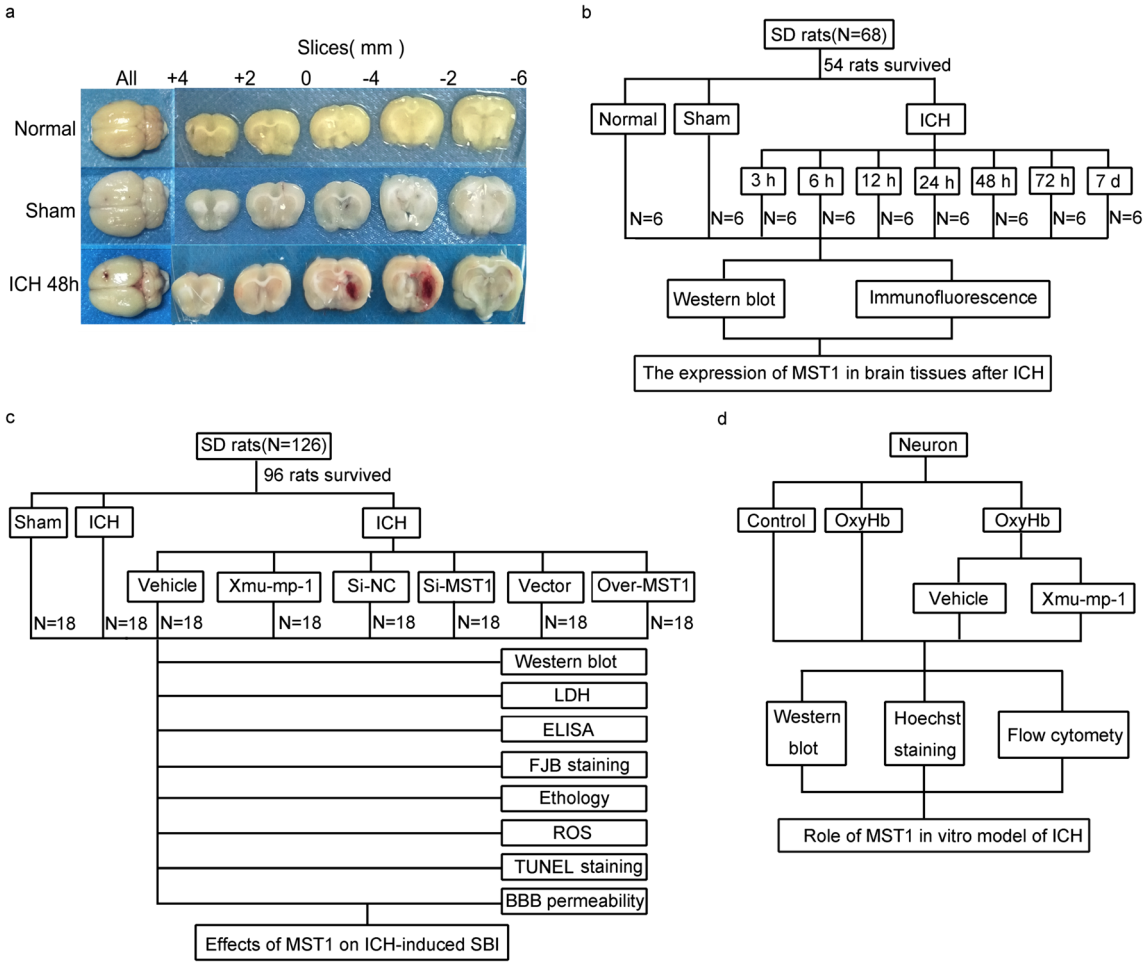

Fig. 1 ICH model and experimental design. **a** Brain coronal sections were shown. **b** Experiment 1 explored the time course of changes in levels of P-MST1 after ICH. **c** Experiment 2 was performed to explore the role of MST1 signaling pathway in SBI after ICH in vivo. **d** Experiment 3 investigated that MST1 was an important factor in inducing neuronal apoptosis in vitro

ICH Model In Vitro

Neuronal-rich cultures were prepared from brain tissues of fetal rats (embryonic days 16–18) [24]. Meninges and blood vessels were removed, and then brain tissues were digested with 0.25% trypsin (containing EDTA) for 5 min at 37 °C. These tissues were washed three times with PBS to stop trypsin digestion. Next, the brain tissue suspension was centrifuged at 1500 rpm for 5 min, and the cells were resuspended in Neurobasal medium containing 2% B27, 2 mM L-glutamine, 50 U/ml penicillin, and 50 U/ml streptomycin (all from Gibco, USA). Finally, cells were plated in six-well plates with fresh medium and half of medium was changed by fresh medium every 2 days. In vitro ICH model was established by stimulation of neurons using oxygen hemoglobin (OxyHb). Neurons were incubated with OxyHb (20 μM) at 37 °C and 5% CO_2 for 6 h. Next, medium was removed; and neurons were washed three times with PBS, and followed by other experiments.

Experimental Design

Before induction of ICH, all rats were numbered and randomly divided into three groups (6 rats to Normal group, 18 rats to Sham group, and the other rats to ICH group), using a table of random numbers by a technician who did not take part in this study. After induction of ICH, all ICH rats were randomly divided into some groups (details were shown below), using the table of random numbers by a technician who did not participate in this study.

Experiment 1: The levels of P-MST1 in brain tissues of rats after ICH. To examine the changes of MST1 and P-MST1 in various time points after ICH, 54 rats (6 rats come from Normal group, 6 rats come from Sham group, and 42 rats were survived surgery, out of an initial 56 rats in ICH group) were randomly divided into nine groups of 6 rats each: Normal group, Sham group, and seven experimental groups were arranged by following time points: 3, 6, 12, 24, 48, 72 h, and 7 days after ICH. All

experimental rats were sacrificed in indicated time points after ICH. For each ICH rat, two brain coronal sections were collected: 3 mm before and 4 mm after coronal injection point, respectively. Then, the right basal ganglia was separated immediately from the 3-mm thickness slice and used for western blot analysis; the 4-mm thickness section was fixed in 4% paraformaldehyde, embedded in paraffin, cut into 4 μm sections, and used for double immunofluorescence analysis (Fig. 1b).

Experiment 2: Effects of MST1on SBI induced by ICH and underlying mechanisms in vivo. In in vivo experiment, 144 rats (18 rats come from Sham group and 126 rats are survived surgery, out of an initial 160 rats in ICH group) were randomly divided into eight groups (18 rats/group): Sham group, ICH group, ICH + Vehicle group, ICH + Xmu-mp-1 group, ICH + Si-negative control (Si-NC) group, ICH + Si-MST1 group, ICH + Vector group, and ICH + Over-MST1 group. At 48 h after ICH, 18 rats were randomly divided two parts: 12 rats were tested for behavioral disturbances and then 6 rats were exsanguinated and their brain tissues were collected as described above for western blot analysis, terminal deoxynucleotidyl transferase-mediated dUTP nick-end labeling (TUNEL) staining, Fluoro-Jade (FJB) staining, and reactive oxygen species (ROS) assays, and the other 6 rats were used to evaluate brain edema; the last 6 rats were used to test BBB injury. In addition, blood samples were collected from 6 rats in each group for serum lactate dehydrogenase (LDH), IL-1β, and TNF-α detection (Fig. 1c).

Experiment 3: Exploration underlying mechanism of the role of MST1 in vitro. In in vitro experiment, primary cultured neurons were used and divided into four groups: Control group, OxyHb group, OxyHb + Vehicle group, and OxyHb + Xmu-mp-1 group (Fig. 1d). The details about each group were described below.

Drug Administration

Xmu-mp-1 (Selleck, China) was prepared in DMSO at the concentration of 0.05 mg/μl [25]. At 2 h before ICH induction, this inhibitor (6 μl to each rat) was injected into lateral ventricle. An equal volume of DMSO was injected and used as Vehicle. In in vitro experiments, Xmu-mp-1 was dissolved in DMSO at the final concentration of 50 μM, and the final concentration of Xmu-mp-1 was 50 nM in the neuron culture medium.

Plasmid and siRNA Transfection in Rat Brain Tissues

Two types of plasmids were used in this study. One plasmid could express rat MST1 in rat brain tissues (Over-MST1; Gene ID: 24566), and the other plasmid was an empty Vector (Vector) as the negative control for Over-MST1. Over-MST1 and Vector (both 1 mg/ml) plasmids were purchased from Genescript (China). They were diluted to 0.5 mg/ml by enhanced transfection solution before intracerebroventricular injection in rats. Plasmid transfection was performed based on the manufacturer's instructions in this study. Ten microliters Entranster-in vivo DNA transfection reagent (Engreen, China) was immediately added to 5 μl plasmid or Vector. These solutions were mixed at room temperature for another 15 min. Finally, 15 μl Entranster-in vivo plasmid mixture was intracerebroventricularly injected to rats at 48 h before ICH induction.

To reduce the level of MST1 expression, a specific siRNAs of MST1 were achieved from GenScript (China). We followed the manufacturer's instructions of Entranster-in vivo RNA transfection reagent (Engreen, China), the siRNA transfection complexes were prepared as follows: briefly, 5 nmol MST1 siRNA was dissolved in 66.5 μl DEPC RNase-free water, and 5 μl Entranster-in vivo RNA transfection reagent was then added to 10 μl diluted MST1siRNA. The solution was mixed at room temperature for 15 min. At last, 15 μl Entranster-in vivo siRNA mixture was intracerebroventricularly injected to rats at 48 h before ICH induction.

Western Blot Analysis

Western blot analysis was performed as a previous study reported [24]. Briefly, the brain samples of rats or extracted neurons were mechanically lysed in a RIPA lysate buffer (Beyotime, China). The protein concentrations were measured by the bicinchoninic acid (BCA) method using a specific assay kit (Beyotime, China). The protein samples (30 μg/lane) were loaded onto a 10% SDS-polyacrylamide gel, separated, and then electrophoretically transferred to a polyvinylidene difluoride (PVDF) membrane (Millipore Corporation, USA). The membrane was blocked with 5% bovine serum albumin (BSA, BioSharp, China) at 25 °C for 1 h. Next, the membrane was incubated with primary antibodies at 4 °C for overnight. The main antibodies used in this study were as follows: P-MST1, MST1, P-YAP, YAP, P-LATS1, Albumin (Cell Signaling Technology, USA), and LATS1 (Abcam, USA). In addition, β-tubulin (Cell Signaling Technology, USA) was served as a loading control. Finally, the membrane was incubated with HRP-conjugated secondary antibody (Cell Signaling Technology, USA) at 25 °C for 1 h. Banding signals were visualized using an Enhanced Chemiluminescence (ECL) kit (Beyotime, China) and the relative amounts of proteins were analyzed by ImageJ software (NIH, USA) and normalized to above Sample control. In addition, phosphorylation levels were assessed as ratio of phosphoprotein to total protein.

Immunofluorescent Staining

In in vivo experiments, brain samples were fixed in 4% paraformaldehyde, embedded in paraffin, and cut into 4 μm sections. Following antigen retrieval and blocking of nonspecific binding, brain sections were incubated with the primary antibody (against P-MST1, Cell Signaling Technology, USA) at 4 °C for overnight and corresponding secondary antibodies (Life Technologies, USA) at 25 °C for another 1 h. At last, brain sections were observed in a fluorescence microscope (Olympus Co., Japan). The relative fluorescence intensity of each image was analyzed by the ImageJ program (NIH, USA). The quantitative analysis was performed by a technician blinded to experimental conditions.

Brain Edema and BBB Injury

As described in a previous report [26], wet-dry method was used to assess brain edema of rats in various groups in this study. Briefly, rats were injected i.p. with 4% chloral hydrate 48 h after ICH induction, and the intact brain removed immediately. The brain was divided into two hemispheres along the midline, and each hemisphere was further dissected into two parts containing the cortex and basal ganglia. The resulting tissue was then subdivided into five samples: contralateral basal ganglia (Cont-BG), contralateral cortex (Cont-CX), cerebellum (CB), ipsilateral basal ganglia (Ipsi-BG), and ipsilateral cortex (Ipsi-CX). These brain samples were immediately weighed with an electronic analytical balance and their wet weights recorded. Tissues samples were then dried at 100 °C for 72 h and weighed again to determine the dry weight. Brain water content was calculated using the formula [(wet weight − dry weight)/wet weight] × 100%.

As described in a previous report [27], to quantify low-molecular-weight molecular leakage, we injected with 2% FITC-dextran (100 μg/ml, 0.2 ml; Sigma-Aldrich, USA) to rats. Two hours later, the rats were subjected to systemic intracardiac perfusion with 1 USP U/ml heparin in saline to flush the FITC-dextran out of the vasculature. Five minutes later, the rats were euthanized, and their perfused brains were subsequently harvested. Supernatant fluorescence was measured using an EnSpire Manager Multimode Plate Reader (PerkinElmer, USA).

Neurobehavioral Evaluation

At 48 h after ICH, 12 rats in each group in experiment 2 were tested for behavioral impairment by a scoring system and were monitored for seven individual tests including spontaneous activity, axial sensation, vibrissae proprioception, symmetry of limb movement, lateral turning, forelimb walking, and climbing as reported previously [28] (details were shown in Table 1).

TUNEL Staining

Cell apoptosis was detected by TUNEL staining based on manufacturer's protocol (Roche, Switzerland). Briefly, the slices were incubated in 0.1% Triton X-100 for 8 min and then washed three times with PBS. Next, they were incubated with TUNEL staining reagents for 1 h at 37 °C. The sections were observed with a fluorescence microscope (Olympus Co, Japan). To quantitate apoptosis, the apoptosis index was defined as the percentage of TUNEL-positive cells in brain tissues of rats.

FJB Staining

FJB is a polyanionic fluorescein derivative, and used to detect the neuronal degradation in this research. Brain sections were deparaffinized, dehydrated, and then incubated in 0.06% potassium permanganate solution (Sigma-Aldrich, USA) for 10 min. Next, these sections were rinsed in deionized water, immersed in FJB working solution (0.1% acetic acid) for 20 min, and dried in an incubator. At last, the sections were cleared in xylene and used anhydrous, low-fluorescence, styryl-based mounting media (DPX, Sigma-Aldrich, USA). The FJB-positive cells were observed by a fluorescence microscopy (Olympus Co, Japan) and counted by a technician blinded to experimental conditions.

ELISA

The concentrations of TNF-α and IL-1β in all serum samples were measured by the specific ELISA kit (Bio-Swamp, China). These measurements were based on the instructions of manufacturer.

ROS Assay

A ROS assay kit (Beyotime, China) was used to test ROS levels in brain tissues of rats in this study. The obtained brain tissues samples were homogenized and centrifuged at 12,000*g*, 4 °C for 10 min; and the superabundant was collected for ROS analysis. Based on the instructions of manufacturer, the ROS concentration was evaluated by oxidant-sensitive probe 2,7-dichlorofluorescein diacetate (DCF-DA). Fluorescence intensity was measured by a fluorometric microplate reader (Molecular Devices, USA) with excitation at 485 nm and emission at 530 nm, respectively. The ROS levels in various experimental groups were expressed as fluorescence intensity/mg protein, and then normalized to the Sham group, which provided relative levels of oxidative stress.

Table 1 Neurobehavioral evaluation: Neuroscore scoring criteria for the sub-tests

Category	Behavior	Score
Spontaneous activity (SA)	Animal was akinesitic	0
	Animal moves slowly or minimally	1
	Animal approached 1–2 walls	2
	Animal approached at least 3 walls of the cage or raised on hindlimbs to explore the top of the cage	3
Vibrissae proprioception (VP)	–	0
	Animal had a unilateral response	1
	Animal had either a weak bilateral response or weak left response and brisk right response	2
	Animal had a brisk bilateral response	3
Axial sensation (AS)	–	0
	Animal had no response on left side	1
	Animal had either a weak bilateral response or weak left response and brisk right response	2
	Animal had a brisk bilateral response	3
Limb symmetry (LS)	Hemiparesis	0
	Left forelimb or left hindlimb flexed	1
	Asymmetric extension	2
	All limbs were extended symmetrically	3
Lateral turning (LT)	Animal had no turning at all on one side	0
	Animal had unequal turning	1
	Animal turned bilaterally less than 45° on both sides	2
	Animal turned bilaterally at least 45° on both sides	3
Forelimb walking (FW)	Animal had a paretic forelimb	0
	Animal walked in circles	1
	Animal walked asymmetrically or to one side	2
	Animal briskly walked symmetrically on forepaws	3
Climbing (CL)	–	0
	Animal failed to climb or circled instead of climbing	1
	Animal climbed to the top and had a weak grip or animal climbed but had a strong grip	2
	Animal climbed to the top and had a strong grip	3

Lactate Dehydrogenase Assay

The concentration of lactate dehydrogenase (LDH) in serum was detected by using a LDH assay kit (Jiancheng Biotech, China). These assays were performed according to instructions of manufacturers, and these data were expressed relative to standard curves prepared for them.

Annexin V and PI Staining In Vitro

Following treatments mentioned above, primary cultured neurons were trypsinized using 0.25% trypsin and then centrifuged at 500*g* for 5 min. The cell pellet was resuspended in 500 μl binding buffer. Then, 5 μl Annexin V and PI (Beyotime, China) were both added to cell suspension. After incubation at 37 °C for 20 min, stained neurons were tested using a flow cytometry (FACS Cabibur, BD, USA) and at least 20,000 events per sample were recorded.

Hoechst Staining In Vitro

Briefly, after various treatments, cultured neurons were fixed with 4% neutral-buffered formaldehyde for 10 min. They were then rinsed with PBS for 5 min and stained using Hoechst working solution for 15 min at 25 °C. The neurons were rinsed again three times in PBS for 5 min each time and analyzed by a fluorescence microscope (Olympus Co., Japan).

Statistical Analysis

All data were presented as mean ± SEM. GraphPad Prism 6.0 software (GraphPad, USA) was used for statistical analysis. Data sets were tested for normality of distribution using the Kolmogorov–Smirnov test. Data groups (two groups) with normal distribution were compared by the two-sided unpaired Student's *t* test, and the Mann–Whitney *U* test was used for nonparametric data. $P < 0.05$ was indicated as a statistically significant difference.

Results

General Observation

We observed that there were no significant differences in body weight, body temperature, blood pressure, and arterial blood gases; glucose of rats in different experimental ICH groups were measured (data not shown). No rats died in Normal group (0/6 rats) and Sham group (0/24 rats), and the mortality rate of the rats with ICH is 22.2% (48/216 rats), and 48 rats died after anesthesia or modeling during the surgery and the mortality rate was not significantly different between the experimental groups. The representative brain coronal sections of rats in Normal group, Sham group, and ICH group were shown in Fig. 1a. There were stable hematoma volumes located in ipsilateral hemispheres of rats in ICH group at 48 h after ICH induction; however, it only had a hemorrhage point in ipsilateral hemispheres of rat induced by the insertion of microsyringe in Sham group at 48 h after induction.

Time Course of Changes in the MST1 Phosphorylation Levels in Brain Tissues After ICH

To detect the phosphorylation levels of MST1 in rat brain tissues around hematoma after ICH, we performed western blot and immnofluorescence analyses. The results of western blot displayed that ICH can lead to the increases in the phosphorylation levels of MST1. The levels of P-MST1 increased significantly as early as 3 h after ICH induction, peaked at 48 h, and then decreased. Moreover, compared with Normal group, Sham group has no statistical differences (Fig. 2a, b). However, we found that total protein levels of MST1 have no significant changes in various time points after ICH

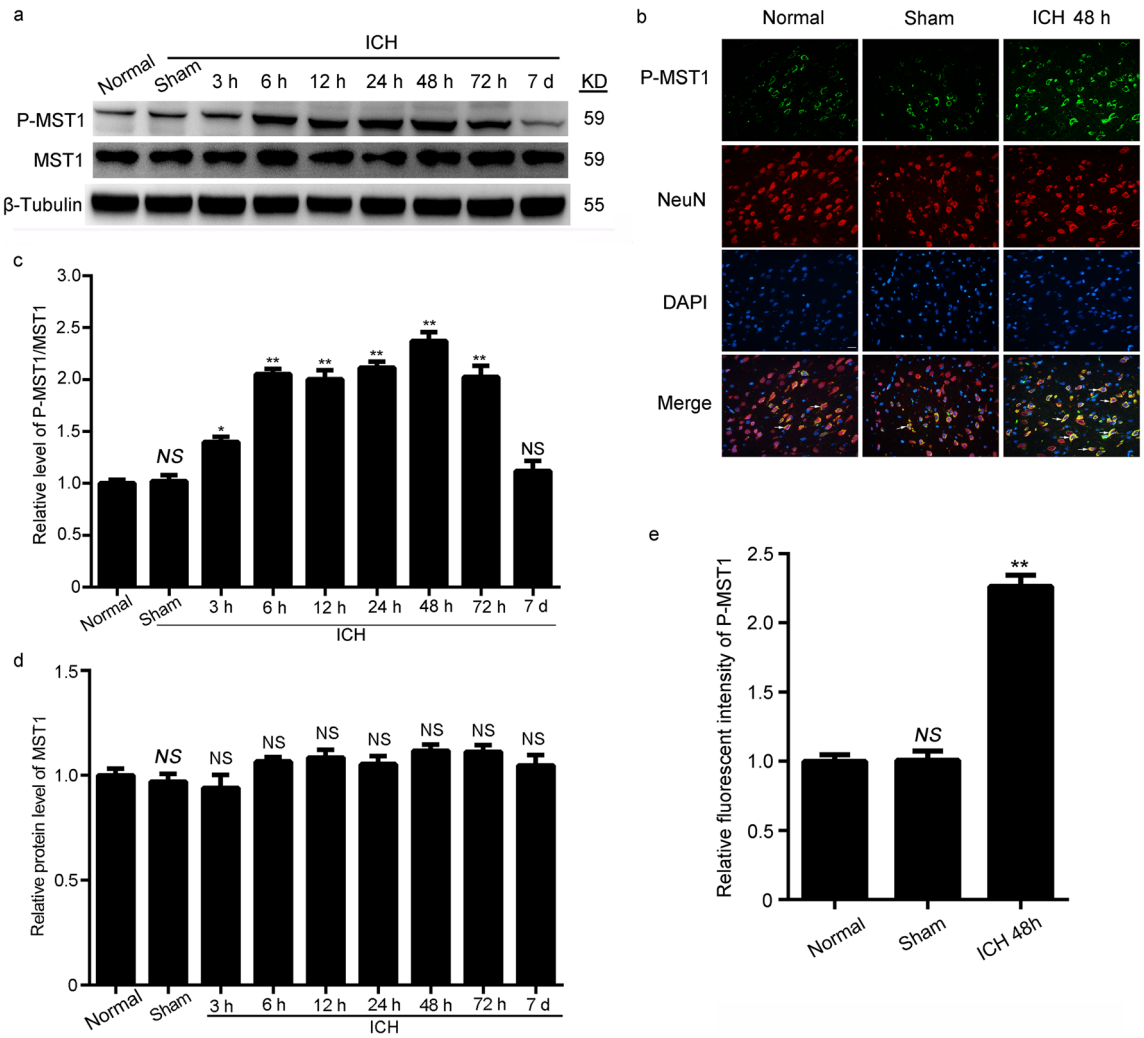

Fig. 2 The levels of P-MST1 and MST1 in brain tissues of rats after ICH. **a** The levels of P-MST1and MST1 at 3 h, 6 h, 12 h, 24 h, 48 h, 72 h, and 7 days after ICH. Quantification of the changes of levels in P-MST1 (**b**) and MST1 (**c**). **d** The P-MST1 (green) and neuron marker (NeuN, red), and nuclei labeled with DAPI (blue) were shown. Arrows indicated P-MST1-positive neurons, Scale bar = 20 μm. **e** The relative fluorescence intensity of P-MST1. All data were displayed as means ± SEM, mean values for Normal group were normalized to 1.0; NS, no significant difference vs. Normal group; $*P < 0.05$, $**P < 0.01$ vs. Sham group; NS, no significant difference vs. Sham group. $n = 6$

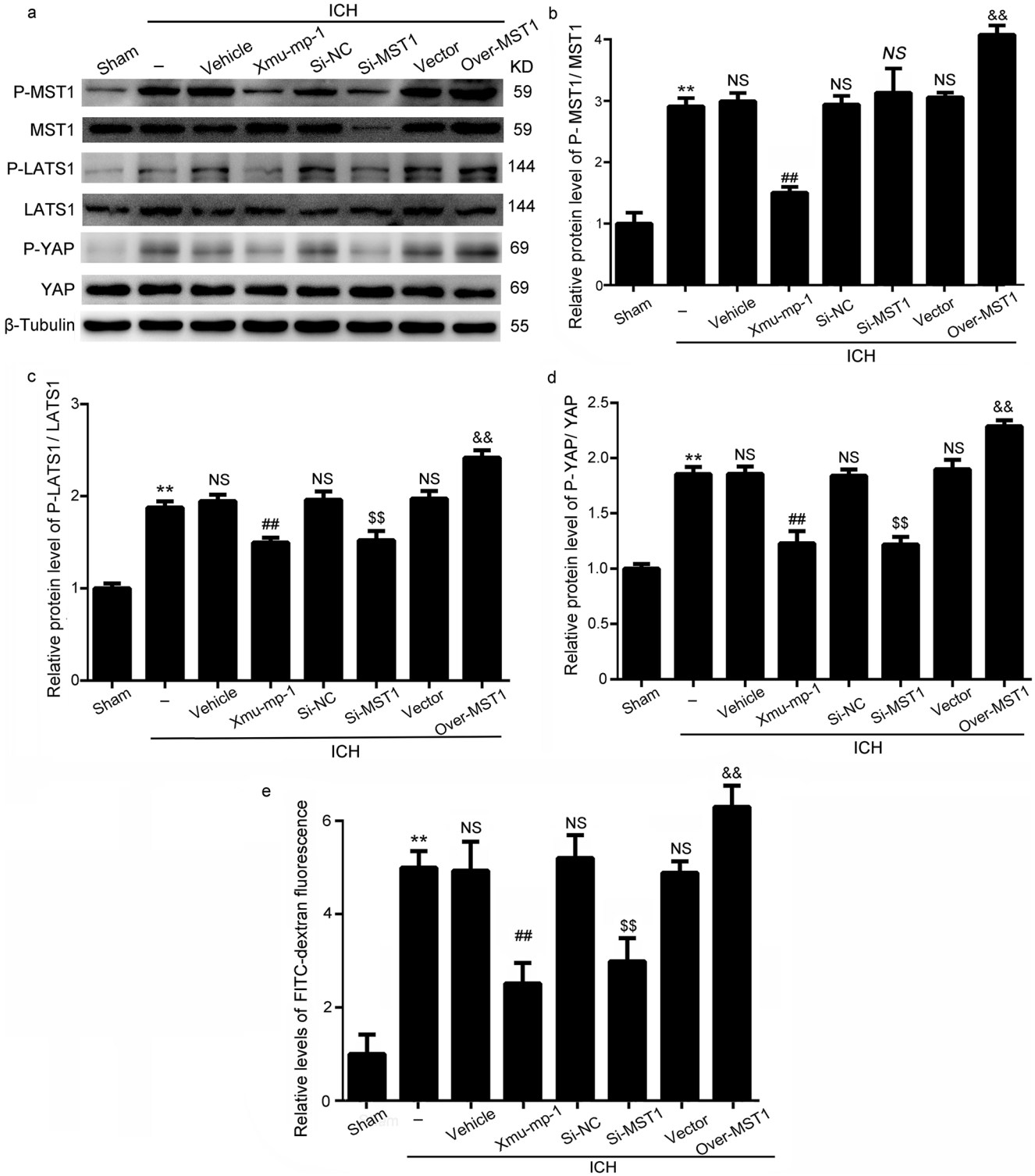

Fig. 3 Knockdown of MST1 level reduced BBB damage in rats after ICH. **a** The levels of P-MST1, P-LATS1, and P-YAP were significantly reduced under the treatments of Xmu-mp-1 and MST1 siRNA. Opposite results were observed in the Over-MST1 group. Quantification of the levels of P-MST1/MST1 (**b**), P-LATS1/LAST1 (**c**), and P-YAP/YAP (**d**) was shown. NS, no significant difference vs. ICH + Si-NC group. **e** The relative level of FITC-dextran fluorescence in each group. All values were means ± SEM, mean values for Sham group were normalized to 1.0; $^{**}P < 0.01$ vs. Sham group; NS, no significant difference vs. ICH group; $^{\#\#}P < 0.01$ vs. ICH + Vehicle group; $^{\$\$}P < 0.01$ vs. ICH + Si-NC group; $^{\&\&}P < 0.01$ vs. ICH + Vector group. $n = 6$

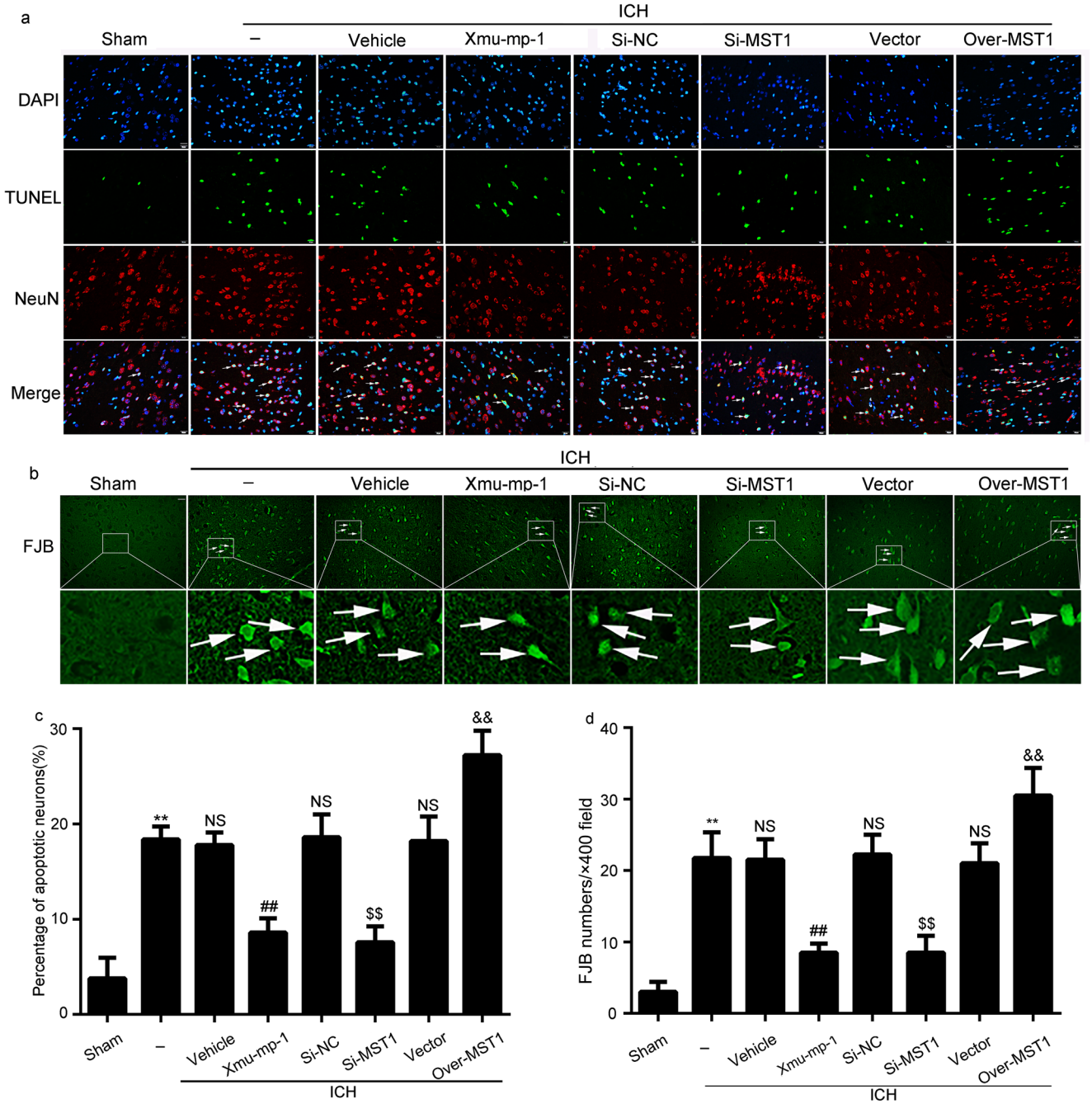

Fig. 4 Deletion and over-expression of MST1 can respectively reduce and increase neuronal apoptosis and degeneration after experimental ICH. **a** TUNEL staining was performed to detect apoptosis in brain tissues after ICH. Arrows indicated NeuN/TUNEL-positive cells. Percentage of TUNEL-positive neurons in various groups was shown in **c**. **b** Fluoro-Jade B (FJB) staining showed neuronal degeneration in cerebral cortex of rats in different groups. Arrows pointed to FJB-positive cells. FJB-positive cells/mm^2 was quantified in brain cortex (**d**). Scale bar = 20 mm. All values were means ± SEM; $^{**}P < 0.01$ vs. Sham group; NS, no significant difference vs. ICH group; $^{\#\#}P < 0.01$ vs. ICH + Vehicle group; $^{\$\$}P < 0.01$ vs. ICH + Si-NC group; $^{\&\&}P < 0.01$ vs. ICH + Vector group. $n = 6$

(Fig. 2a, c). Immunofluorescence assay further verified that P-MST1-positive cells were co-localized with NeuN-positive cells, which indicated that increased phosphorylation of MST1 mainly occurred in neurons after ICH (Fig. 2d, e). Based on these results, the following experiments were performed at 48 h after ICH.

Increased P-MST1 Activated the Hippo Signaling Pathway and Increased BBB Injury, Neuronal Apoptosis, and Degeneration in Rats After ICH

To further examine the role of P-MST1 in SBI induced by ICH, we regulated the protein levels of MST1 using chemical

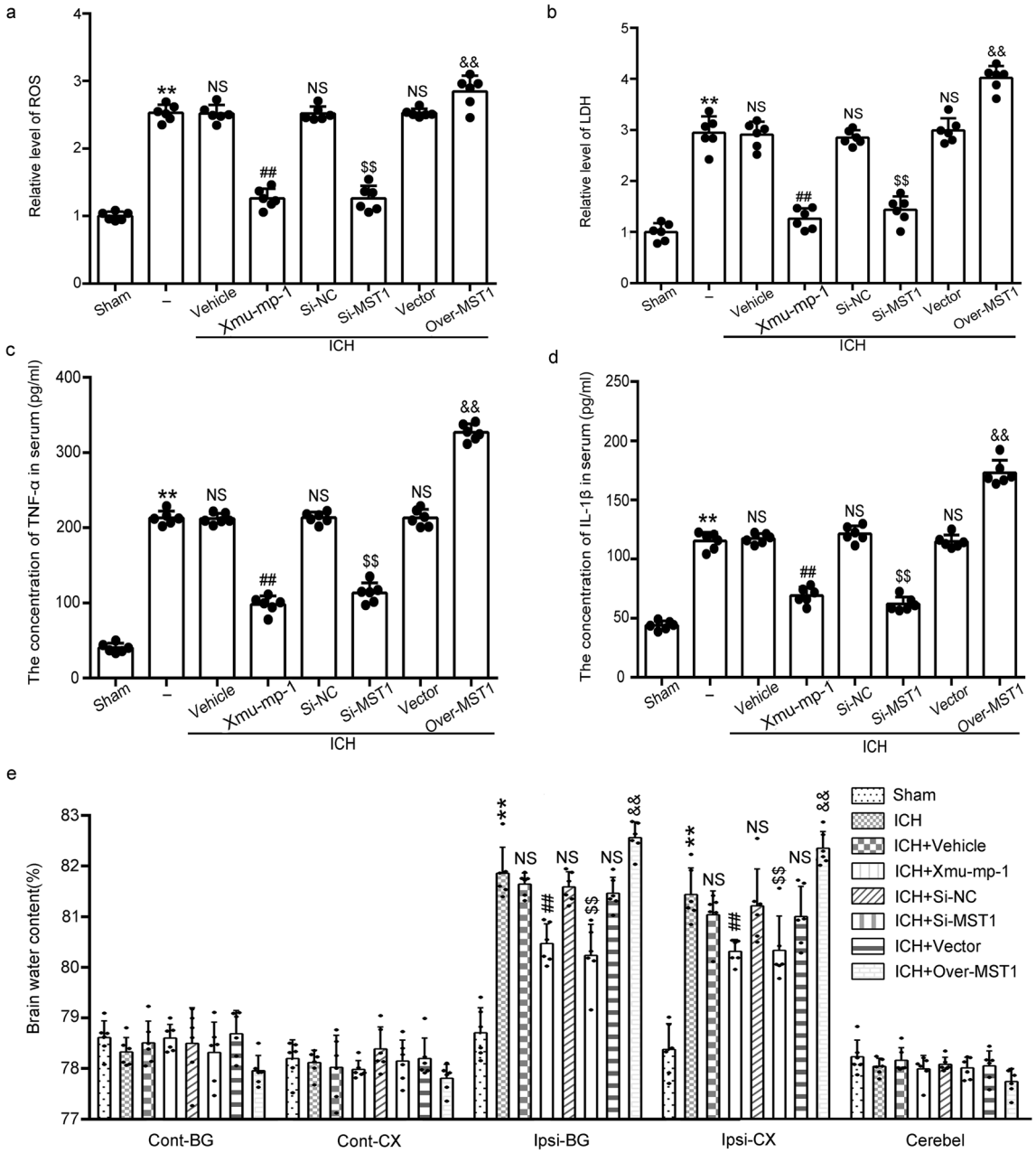

Fig. 5 The role of MST1 signaling pathway in SBI after ICH in vivo. **a** The levels of ROS in the brain tissues in different groups. **b** The levels of LDH in the serum of rats in different groups. **c** The levels of TNF-α in the serum of rats in different groups. **d** The levels of IL-β in the serum of rats in various groups. **e** Brain water content was decreased in the ICH + Si-MST1 and ICH + Xmu-mp-1 group, whereas it was opposite in the ICH + Over-MST1 group both in Ipsi-CX and Ipsi-BG. All values were means ± SEM, and mean values for Sham group were normalized to 1.0. The black dots represented individual data in each group. $^{**}P < 0.01$ vs. Sham group; NS, no significant difference vs. ICH group; $^{\#\#}P < 0.01$ vs. ICH + Vehicle group; $^{\$\$}P < 0.01$ vs. ICH + Si-NC group; $^{\&\&}P < 0.01$ vs. ICH + Vector group. $n = 6$

inhibitor, genetic knockdown, and over-expression in brain tissues of rats. First, we used drug intervention by Xum-mp-1 (a specific antagonistic of P-MST1). Second, we performed genetic knockdown by small interfering RNA (siRNA) and over-expression using plasmid transfection of MST1 in rat model of ICH. The results of western blot analysis showed that, compared with Sham group, the levels of LATS1 phosphorylation and YAP phosphorylation were significantly increased in ICH group. Inhibition and knockdown of MST1 phosphorylation significantly decreased the levels of LATS1 phosphorylation and YAP phosphorylation, while over-expression of MST1 exerted opposite results. There were no significant changes in phosphorylations of LATS1 and YAP in ICH + Vehicle group, ICH + Si-NC group, and ICH + Vector group when compared to the ICH group (Fig. 3a–d). In addition, FITC-dextran is commonly used to measure BBB permeability; it was used in the present study.

Table 2 Clinical behavior scores in each group ($n = 12$)

Group	Score (mean ± SEM)
Sham	19.08 ± 0.4516
ICH	5.083 ± 0.3362[a]
ICH + Vehicle	5.167 ± 0.3445[b]
ICH + Xmu-mp-1	11.67 ± 0.4820[c]
ICH + Si-NC	4.917 ± 0.3786[d]
ICH + Si-MST1	11.92 ± 0.5430[e]
ICH + Vector	5.333 ± 0.3553[f]
ICH + Over-MST1	3.667 ± 0.2247[g]

[a] $P < 0.01$ vs. Sham group
[b] $P > 0.05$ vs. ICH group
[c] $P < 0.01$ vs. ICH + Vehicle group
[d] $P > 0.05$ vs. ICH group
[e] $P < 0.01$ vs. ICH + Si-NC group
[f] $P > 0.05$ vs. ICH group
[g] $P < 0.01$ vs. ICH + Vector group

These results indicated that there was a higher level of FITC-dextran fluorescence in ICH group compared with Sham group; MST1 inhibition and knockdown in ICH rats could reduce BBB injury, while over-expression of MST1 showed opposite results (Fig. 3e). To explore the role of MST1 in neuronal cell death and degeneration in brain tissues after ICH, we performed TUNEL and FJB staining. TUNEL staining showed that the numbers of apoptotic neurons were significantly reduced in the Xum-mp-1 and Si-MST1 treatment groups, while the over-expression of MST1 produced opposite results (Fig. 4a, c). These results suggested that a decrease in P-MST1 can reduce neuronal cell death during ICH. Consistently, FJB staining showed that the numbers of FJB-positive cells increased in ICH group when compared to Sham group. The number of FJB-positive cells increased significantly following the over-expression of MST1 treatment, while there was no obviously difference in ICH + Vector group. In contrast, downregulation of MST1 led to lower ratio of FJB-positive neurons (Fig. 4b, d). These results indicated that MST1 augmented ICH-induced neuronal degeneration via regulated LATS1 phosphorylation and YAP phosphorylation in ICH rats.

Knockdown of MST1 Level Reduced Oxidative Stress, Inflammatory Response, and Brain Edema in Rats After ICH

To further explored potential mechanism of MST1-modulated neuronal dysfunction and the role MST1 in inflammation and oxidative stress, we assessed the levels of TNF-α and IL-β,

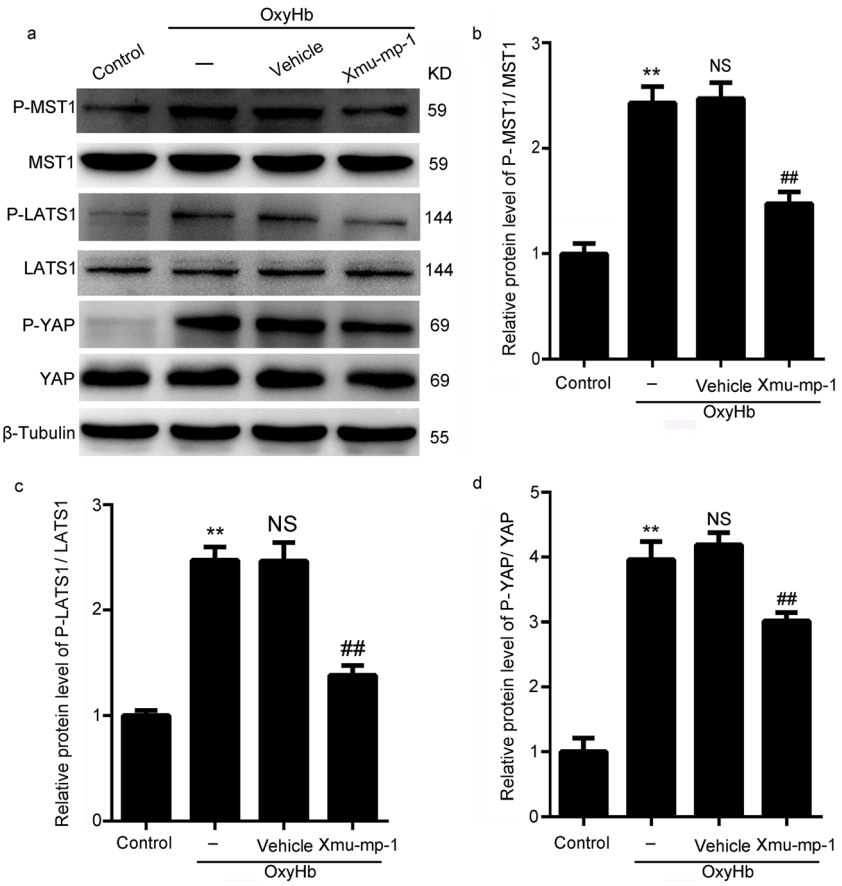

Fig. 6 Effects of Xmu-mp-1 on the levels of P-MST1 and its downstream protein in vitro. **a** The levels of P-MST1 and its downstream protein after Xmu-mp-1 treatment in an in vitro model of ICH. Quantification of the levels of P-MST1/MST1 (**b**), P-LATS1/LAST1 (**c**), and P-YAP/YAP (**d**) was shown. All values were means ± SEM, and mean values for Control group were normalized to 1.0. $^{**}P < 0.01$ vs. Control group; NS, no significant difference vs. OxyHb group; $^{\#\#}P < 0.01$ vs. OxyHb + Vehicle group. $n = 3$

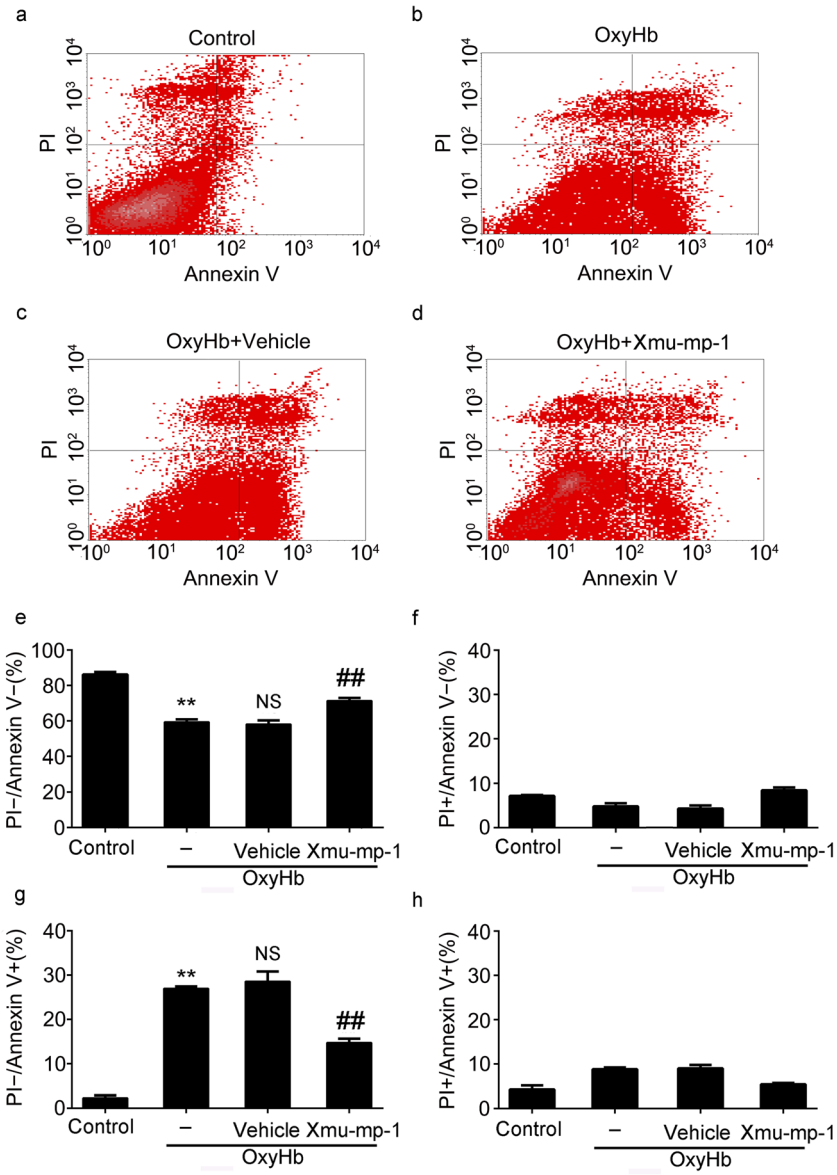

Fig. 7 Xmu-mp-1treatment reduced neuronal apoptosis in vitro. **a–d** The apoptosis of neurons were detected by PI and Annexin V staining and flow cytometry analysis in vitro, PI −/Annexin V+ represented apoptotic neurons. The results of flow cytometry were analyses in (**e–h**). All values were means ± SEM. $^{**}P < 0.01$ vs. Control group; NS, no significant difference vs. OxyHb group; $^{\#\#}P < 0.01$ vs. OxyHb + Vehicle group. $n = 3$

ROS and LDH. Compared with Sham group, the levels of ROS in brain tissues and LDH in serum were increased in ICH group. Especially, over-expression of MST1 obviously elevated the levels of ROS and LDH, while Vector treatment resulted in no obviously changes. However, MST1 knockdown treatment produced the opposite results (Fig. 5a, b). These results suggested that MST1 knockdown could inhibit oxidative stress and neuronal damage induced by ICH. The results of TNF-α and IL-β assays were consistent with these findings (Fig. 5c, d). To examine the effect of MST1 on brain edema after experimental ICH, brain water content was detected using wet/dry weight method. The results suggested that, compared with ICH group, brain water content was significantly reduced in the MST1 inhibition and knockdown groups, while over-expression of MST1 deteriorated brain edema. Taken together, these data indicated that reduction of MST1 can relieve brain edema in rats after ICH.

Inhibition and Knockdown of MST1 Attenuated Neurobehavioral Damage and Cognitive Dysfunction in Rats After ICH

Brain injury is often accompanied by different degrees of neurobehavioral impairment. Our experiments demonstrated that the rats in ICH group had severe neurobehavioral impairment when compared to Sham group. However, the neurobehavioral impairment of the MST1 siRNA and Xum-mp-1 groups was significantly improved compared with ICH group. In contrast, the MST1 over-expression group showed an opposite result (Table 2). These results suggested that MST1 may be involved in the pathological process after ICH.

Effects of Xum-mp-1 on the Hippo Signaling Pathway and Neuronal Apoptosis In Vitro

To further explore the mechanism of Hippo signaling pathway in ICH, an in vitro model of ICH was used in our study: oxygen hemoglobin (OxyHb) to deal directly with the neurons. The result showed that the level of P-MST1 increased in cultured neurons treated with OxyHb when compared to Control group and the phosphorylations of LATS1 and YAP were also increased accordingly. However, inhibition of P-MST1 by treatment with Xmu-mp-1 reduced obviously the phosporylations of LATS1 and YAP (Fig. 6a–d). These results were consistent with those in the in vivo experiments. To further certify the role of MST1 on neuronal apoptosis in vitro, we performed Annexin V and PI staining and Hoechst staining. The results of Annexin V and PI staining showed that apoptotic cells were increased obviously in OxyHb group compared with Control group, while significantly reduced by Xmu-mp-1 treatment (Fig. 7a–h). The results of Hoechst staining suggested that compared with Control group, the apoptosis rate of neurons directly stimulated by OxyHb was higher, whereas there was a lower apoptosis ratio in Xmu-mp-1 treatment group (Fig. 8a, b).These results indicated that MST1 may participate in the neuronal apoptosis after ICH.

Discussion

ICH can cause a series of biological reactions, such as inflammation and cell death in injured perihematomal tissues [4]. The initial factors of apoptosis include decreased blood flow and reduced metabolism around the hematoma, activation of various enzymes in blood, and mechanical damage of the hematoma after ICH [29–31]. The purpose of this study was to analyze the effects of MST1 on ICH-induced SBI. In present study, we found that the level of P-MST1 in brain tissues under normal condition is low, but rapidly increased after ICH. Analyzing the time course of MST1 phosphorylation levels in brain tissues after ICH, the results showed that the levels of P-MST1 significantly increased starting from 3 h and peaked at 48 h after ICH. It has already been reported that the protein kinase Src phosphorylates MST1 after ICH, which can trigger stabilization and activation of MST1 [17, 22]. We also investigated the role and underlying mechanism of MST1-mediated SBI induced ICH through intervention on MST1. We downregulated the levels of P-MST1 by treatment with Xmu-mp-1 (a P-MST1 inhibitor) and silenced the MST1 gene. We found that reducing of P-MST1 reduced neuronal death in the injured area, improved BBB permeability, decreased cerebral edema, and attenuated effectively relieved neurobehavioral disturbance after ICH. In contrast, overexpression of MST1 had an opposite effect. Based on these findings, we inferred a series of biological reactions after ICH. MST1 was phosphorylated and activated in brain tissues after ICH, phosphorylated MST1 activated LATS1/2, LATS1/2 kinases then phosphorylated and inhibited the transcription coactivators YAP and TAZ which were two major downstream effectors of the Hippo signaling pathway [21]. After phosphorylated, YAP/TAZ translated out of the nucleus, which led to YAP/TAZ degradation. Subsequently, cell apoptosis was initiated, which eventually contributed to brain injury [21].

Cell death is a leading cause of brain damage after ICH. Almost prior research suggested that the form of cell death is apoptosis of brain tissues after ICH [29, 30]. As previously

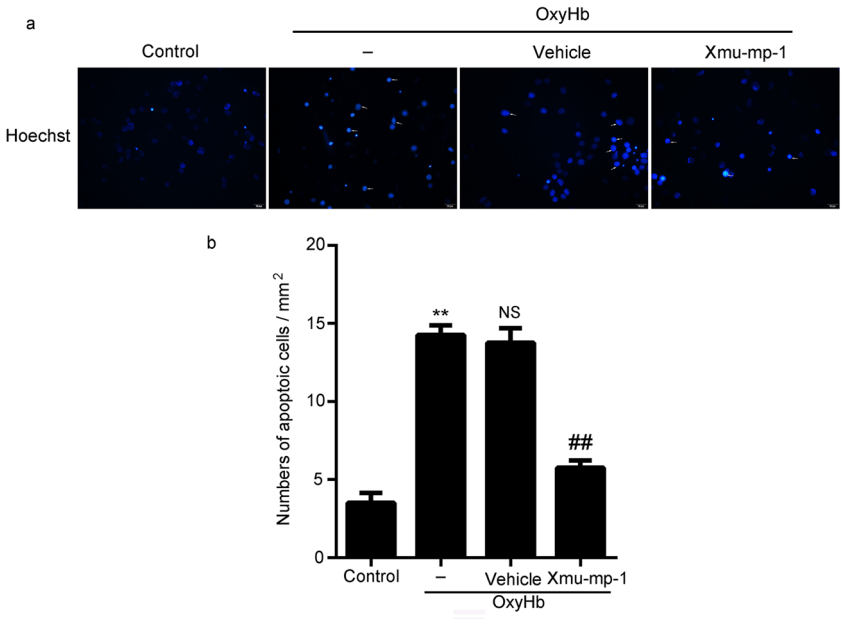

Fig. 8 **a** Hoechst staining was used in detection of neuronal apoptosis in vitro. Arrows indicated Hoechst-positive neurons, Scale bar = 20 mm. **b** Numbers of Hoechst-positive cells. All values were means ± SEM. $^{**}P < 0.01$ vs. Control group; NS, no significant difference vs. OxyHb group; $^{\#\#}P < 0.01$ vs. OxyHb + Vehicle group. $n = 3$

reported, MST1 was involved in apoptosis by phosphorylation of downstream histone H2B and some other related proteins [32, 33]. In addition, it was also reported that oxidative stress induced c-Abl-dependent tyrosine phosphorylation of MST1 and increased the interaction between MST1 and Forkhead box O3 (FOXO3), thus activated the MST1-FOXO signaling pathway, and led to death of primary cultured neurons and rat brain cells [16, 17]. In present study, deletion of MST1 reduced the levels of its two downstream signaling molecules, P-LATS1 and P-YAP, after ICH, which suggested that deficiency of P-MST1 alleviated apoptosis of neurons in ICH. In addition to the apoptosis signaling pathway, damaged brain tissues after ICH were associated with brain edema, oxidative stress, disruption of neurobehavioral function, and so on [34]. Another report displayed that inhibition of MST1 expression can effectively reduce neurological deficits during cerebral ischemia-reperfusion injury [19]. In our study, reduction in P-MST1 levels can mitigate neurological impairment, BBB damage, brain edema, and oxidative stress in ICH rats. As previously reported, MST1 participated in neuronal apoptosis, but the regulatory mechanism of MST1 remained to be determined. In a recent study using a cerebral ischemia model, MST1 activated inflammatory cytokines such as TNF-α and IL-6, which caused inflammation and cell death through Src-MST1-IκB signaling pathway [19, 35]. After TBI, MST1 was phosphorylated and activated, which promoted the transcription of caspase 3, caused neuronal damage and DNA fragmentation, and finally led to neuronal cell death [20]. MST1 phosphorylated Ser14 residues in the BH4 domain of Bcl-xL on the extracellular mitochondrial membrane of myocardial cells, which induced dissociation of Bcl-xL of B cell leukemia/lymphoma 2-related (Bcl-2 related) protein X and promoted apoptosis by activating Bax gene [36]. In the nucleus, MST1 formed a complex with LATS2 and NF2, thus blocking the positive regulation of YAP on the transcription of the pro-survival gene and leading to cell death [37].

Several limitations of this study should be noted. Firstly, although Xmu-mp-1 is a selective MST1 antagonist, it may have antagonistic effects on other members of MST family. Therefore, we also used MST1 siRNA to confirm our results. Secondly, only male rats were used in our study. Thirdly, we only studied MST1-mediated early brain injury after ICH, while its role in late-stage brain injury is not yet clear, further research is required to explore this potential role and mechanism.

In summary, all these results supported potential clinical value of MST1 in treatment of brain injury after ICH. Our experimental results demonstrated the MST1/Hippo signaling pathway exerted an important effect on inducing neuronal apoptosis in SBI after ICH. Inhibition of MST1 can successfully inhibit neuronal MST1-induced apoptosis, reduce brain edema and BBB injury, and improve neurological function.

Funding This study was funded by the National Key R&D Program of China (No. 2018YFC1312600 and 2018YFC1312601), Project of Jiangsu Provincial Medical Innovation Team (No. CXTDA2017003), Jiangsu Provincial Medical Youth Talent (No. QNRC2016728), Suzhou Key Medical Centre (No. Szzx201501), Scientific Department of Jiangsu Province (No. BE2017656), and Suzhou Government (LCZX201601).

Compliance with Ethical Standards

Conflict of Interest The authors declare that they have no conflict of interest.

Ethical Approval All applicable international, national, and/or institutional guidelines for the care and use of animals were followed. This article does not contain any studies with human participants performed by any of the authors.

Informed Consent None.

References

1. Joseph MJ, Caliaperumal J, Schlichter LC. After intracerebral hemorrhage, oligodendrocyte precursors proliferate and differentiate inside white-matter tracts in the rat striatum. Transl Stroke Res. 2016;7(3):192–208.
2. Behrouz R. Re-exploring tumor necrosis factor alpha as a target for therapy in intracerebral hemorrhage. Transl Stroke Res. 2016;7(2):93–6.
3. Dang G, Yang Y, Wu G, Hua Y, Keep RF, Xi G. Early erythrolysis in the hematoma after experimental intracerebral hemorrhage. Transl Stroke Res. 2017;8(2):174–82.
4. Bobinger T, Burkardt P, Huttner HB, Manaenko A. Programmed cell death after intracerebral hemorrhage. Curr Neuropharmacol. 2017.
5. Urday S, Kimberly WT, Beslow LA, Vortmeyer AO, Selim MH, Rosand J, et al. Targeting secondary injury in intracerebral haemorrhage—perihaematomal oedema. Nat Rev Neurol. 2015;11(2):111–22.
6. Xi G, Strahle J, Hua Y, Keep RF. Progress in translational research on intracerebral hemorrhage: is there an end in sight? Prog Neurobiol. 2014;115:45–63.
7. Babel I, Barderas R, Diaz-Uriarte R, Moreno V, Suarez A, Fernandez-Acenero MJ, et al. Identification of MST1/STK4 and SULF1 proteins as autoantibody targets for the diagnosis of colorectal cancer by using phage microarrays. Mol Cell Proteomics. 2011;10(3):M110 001784.
8. Chao Y, Wang Y, Liu X, Ma P, Shi Y, Gao J, et al. Mst1 regulates glioma cell proliferation via the AKT/mTOR signaling pathway. J Neuro-Oncol. 2015;121(2):279–88.
9. Sciarretta S, Zhai P, Maejima Y, Del Re DP, Nagarajan N, Yee D, et al. mTORC2 regulates cardiac response to stress by inhibiting MST1. Cell Rep. 2015;11(1):125–36.
10. Zhang M, Zhang L, Hu J, Lin J, Wang T, Duan Y, et al. MST1 coordinately regulates autophagy and apoptosis in diabetic cardiomyopathy in mice. Diabetologia. 2016;59(11):2435–47.
11. Zhou D, Zhang Y, Wu H, Barry E, Yin Y, Lawrence E, et al. Mst1 and Mst2 protein kinases restrain intestinal stem cell proliferation and colonic tumorigenesis by inhibition of Yes-associated protein (Yap) overabundance. Proc Natl Acad Sci U S A. 2011;108(49):E1312–20.

12. Harvey KF, Pfleger CM, Hariharan IK. The Drosophila Mst ortholog, hippo, restricts growth and cell proliferation and promotes apoptosis. Cell. 2003;114(4):457–67.
13. Udan RS, Kango-Singh M, Nolo R, Tao C, Halder G. Hippo promotes proliferation arrest and apoptosis in the Salvador/Warts pathway. Nat Cell Biol. 2003;5(10):914–20.
14. Wu S, Huang J, Dong J, Pan D. Hippo encodes a Ste-20 family protein kinase that restricts cell proliferation and promotes apoptosis in conjunction with salvador and warts. Cell. 2003;114(4):445–56.
15. Lee JK, Shin JH, Hwang SG, Gwag BJ, McKee AC, Lee J, et al. MST1 functions as a key modulator of neurodegeneration in a mouse model of ALS. Proc Natl Acad Sci U S A. 2013;110(29):12066–71.
16. Lehtinen MK, Yuan Z, Boag PR, Yang Y, Villen J, Becker EB, et al. A conserved MST-FOXO signaling pathway mediates oxidative-stress responses and extends life span. Cell. 2006;125(5):987–1001.
17. Xiao L, Chen D, Hu P, Wu J, Liu W, Zhao Y, et al. The c-Abl-MST1 signaling pathway mediates oxidative stress-induced neuronal cell death. J Neurosci. 2011;31(26):9611–9.
18. Xie Q, Hao Y, Tao L, Peng S, Rao C, Chen H, et al. Lysine methylation of FOXO3 regulates oxidative stress-induced neuronal cell death. EMBO Rep. 2012;13(4):371–7.
19. Zhao S, Yin J, Zhou L, Yan F, He Q, Huang L, et al. Hippo/MST1 signaling mediates microglial activation following acute cerebral ischemia-reperfusion injury. Brain Behav Immun. 2016;55:236–48.
20. Li D, Ni H, Rui Q, Gao R, Chen G. Deletion of Mst1 attenuates neuronal loss and improves neurological impairment in a rat model of traumatic brain injury. Brain Res. 2018;1688:15–21.
21. Meng Z, Moroishi T, Guan KL. Mechanisms of Hippo pathway regulation. Genes Dev. 2016;30(1):1–17.
22. Liu DZ, Sharp FR. The dual role of SRC kinases in intracerebral hemorrhage. Acta Neurochir Suppl. 2011;111:77–81.
23. Deinsberger W, Vogel J, Kuschinsky W, Auer LM, Boker DK. Experimental intracerebral hemorrhage: description of a double injection model in rats. Neurol Res. 1996;18(5):475–7.
24. Shen H, Chen Z, Wang Y, Gao A, Li H, Cui Y, et al. Role of neurexin-1beta and neuroligin-1 in cognitive dysfunction after subarachnoid hemorrhage in rats. Stroke. 2015;46(9):2607–15.
25. Fan F, He Z, Kong LL, Chen Q, Yuan Q, Zhang S, et al. Pharmacological targeting of kinases MST1 and MST2 augments tissue repair and regeneration. Sci Transl Med. 2016;8(352):352ra108.
26. Wang Z, Zhou F, Dou Y, Tian X, Liu C, Li H, et al. Melatonin alleviates intracerebral hemorrhage-induced secondary brain injury in rats via suppressing apoptosis, inflammation, oxidative stress, DNA damage, and mitochondria injury. Transl Stroke Res. 2017.
27. Wu F, Chen Z, Tang C, Zhang J, Cheng L, Zuo H, et al. Acid fibroblast growth factor preserves blood-brain barrier integrity by activating the PI3K-Akt-Rac1 pathway and inhibiting RhoA following traumatic brain injury. Am J Transl Res. 2017;9(3):910–25.
28. Chen S, Zhao L, Sherchan P, Ding Y, Yu J, Nowrangi D, et al. Activation of melanocortin receptor 4 with RO27-3225 attenuates neuroinflammation through AMPK/JNK/p38 MAPK pathway after intracerebral hemorrhage in mice. J Neuroinflammation. 2018;15(1):106.
29. Sukumari-Ramesh S, Alleyne CH Jr, Dhandapani KM. The histone deacetylase inhibitor suberoylanilide hydroxamic acid (SAHA) confers acute neuroprotection after intracerebral hemorrhage in mice. Transl Stroke Res. 2016;7(2):141–8.
30. Delgado P, Cuadrado E, Rosell A, Alvarez-Sabin J, Ortega-Aznar A, Hernandez-Guillamon M, et al. Fas system activation in perihematomal areas after spontaneous intracerebral hemorrhage. Stroke. 2008;39(6):1730–4.
31. Ke K, Rui Y, Li L, Zheng H, Xu W, Tan X, Cao J, Wu X, Cui G, Cao M: Upregulation of EHD2 after intracerebral hemorrhage in adult rats. J Mol Neurosci : *MN* 2014, 54(2):171–180.
32. Cheung WL, Ajiro K, Samejima K, Kloc M, Cheung P, Mizzen CA, et al. Apoptotic phosphorylation of histone H2B is mediated by mammalian sterile twenty kinase. Cell. 2003;113(4):507–17.
33. Vichalkovski A, Gresko E, Cornils H, Hergovich A, Schmitz D, Hemmings BA. NDR kinase is activated by RASSF1A/MST1 in response to Fas receptor stimulation and promotes apoptosis. Curr Biol. 2008;18(23):1889–95.
34. Aronowski J, Zhao X. Molecular pathophysiology of cerebral hemorrhage: secondary brain injury. Stroke. 2011;42(6):1781–6.
35. Herrmann O, Baumann B, de Lorenzi R, Muhammad S, Zhang W, Kleesiek J, et al. IKK mediates ischemia-induced neuronal death. Nat Med. 2005;11(12):1322–9.
36. Nakamura M, Zhai P, Del Re DP, Maejima Y, Sadoshima J. Mst1-mediated phosphorylation of Bcl-xL is required for myocardial reperfusion injury. JCI Insight. 2016;1(5).
37. Mia MM, Chelakkot-Govindalayathil AL, Singh MK. Targeting NF2-Hippo/Yap signaling pathway for cardioprotection after ischemia/reperfusion injury. Ann Transl Med. 2016;4(24):545.